Dissociation of broadband high-frequency activity and neuronal firing in the neocortex

Marcin Leszczyński[1,2*], Annamaria Barczak[2], Yoshinao Kajikawa[2], Istvan Ulbert[3], Arnaud Y. Falchier[2], Idan Tal[1,2], Saskia Haegens[1,4], Lucia Melloni[5], Robert T. Knight[6] and Charles E. Schroeder[1,2*]

[1] Cognitive Science and Neuromodulation Program, Department of Neurological Surgery, Columbia University College of Physicians and Surgeons, New York, New York, USA

[2] Translational Neuroscience Division of the Center for Biomedical Imaging and Neuromodulation, Nathan Kline Institute, Orangeburg, New York, USA

[3] Institute for Psychology of the Hungarian Academy of Sciences, Budapest, Hungary

[4] Donders Institute for Brain, Cognition and Behaviour, Radboud University Nijmegen, Nijmegen, The Netherlands

[5]Department of Neurology, New York University Langone Medical Center, New York, New York, USA

[6]Department of Psychology and the Helen Wills Neuroscience Institute, University of California at Berkeley

*Correspondence to

Marcin Leszczyński & Charles E. Schroeder

Department of Neurological Surgery

Columbia University College of Physicians and Surgeons, 650 West 168 Street, P&S 5-447,

New York, NY 10032

Email: leszczynski.marcin@gmail.com; cs2388@columbia.edu

Broadband High-frequency Activity (BHA; 70-150 Hz), also known as "high gamma," a key analytic signal in human intracranial recordings is often assumed to reflect local neural firing (multiunit activity; MUA). Accordingly, BHA has been used to study neuronal population responses in auditory (1,2), visual (3,4), language (5), mnemonic processes (6-9) and cognitive control (10,11). BHA is arguably the electrophysiological measure best correlated with the Blood Oxygenation Level Dependent (BOLD) signal in fMRI (12-13). However, beyond the fact that BHA correlates with neuronal spiking (12, 14-16), the neuronal populations and physiological processes generating BHA are not precisely defined. Although critical for interpreting intracranial signals in human and non-human primates, the precise physiology of BHA remains unknown. Here, we show that BHA dissociates from MUA in primary visual and auditory cortex. Using laminar multielectrode data in monkeys, we found a bimodal distribution of stimulus-evoked BHA across depth of a cortical column: an early-deep, followed by a later-superficial layer response. Only, the early-deep layer BHA had a clear local MUA correlate, while the more prominent superficial layer BHA had a weak or undetectable MUA correlate. In many cases, particularly in V1 (70%), supragranular sites showed strong BHA in lieu of any detectable increase in MUA. Due to volume conduction, BHA from both the early-deep and the later-supragranular generators contribute to the field potential at the pial surface, though the contribution may be weighted towards the late-supragranular BHA. Our results demonstrate that the strongest generators of BHA are in the superficial cortical layers and show that the origins of BHA include a mixture of the neuronal action potential firing and dendritic processes separable from this firing. It is likely that the typically-recorded BHA signal emphasizes the latter processes to a greater extent than previously recognized.

We investigated the neural mechanisms generating BHA signal and their relationship to MUA in neocortex by analyzing field potential and concomitant MUA signals recorded with laminar multielectrodes in macaque primary visual (V1: 2 animals, 104 experimental sessions) and auditory

(A1: 2 animals, 26 experimental sessions) cortices. We used first and second derivative (current source density or "CSD") analyses of the laminar field potential profiles along with concomitant MUA to localize the neuronal generators of BHA and to determine their spatiotemporal relationship to neuronal firing. Figure 1 displays representative laminar activity profiles recorded from primary visual and auditory cortices. As noted previously (17-20), CSD and MUA profiles in V1 and A1 conform to a feed-forward pattern, with initial excitation (i.e., current sink with concomitant MUA) in Layer L4 (Fig. 1), followed by activation of the extragranular layers. The notion that BHA reflects neuronal firing, raises the obvious prediction that BHA and MUA should have the same spatial and temporal distributions across cortical layers. Contrary to this prediction, however, the spatiotemporal profiles of BHA and MUA were reliably different. In fact, we observed two temporally and spatially distinct BHA components including "early-deep" BHA localized to the infra- and granular layers and "late-superficial" BHA observed in the supragranular layers (Fig. 1e-f). Early-deep BHA had clear spatiotemporal overlap with granular and infragranular MUA, however, the spatio-temporal relation between late-superficial BHA and MUA was much less clear. In fact, late-superficial BHA often had little or no MUA correlate, particularly in V1. Quantitative analyses further support the dissociation of BHA and MUA.

First, consistent with earlier work (12,14-16), we found that while MUA and BHA were significantly correlated at all cortical depths in both V1 and A1 (all Spearman's rho > 0.76; all $p < 0.01$). Correlation profiles however, were nonuniform across layers. Specifically, coefficients in supragranular layers peaked at substantial lags relative to those in deeper layers (9/3.25, 1/-0.5, 2.5/-0.25 ms median for supra-, granular and infragranular layers in V1 and A1, respectively; both Kruskal-Wallis (KW) tests, $p < 0.01$; Fig. 1 b,d). To understand this divergence, we quantified the laminar/temporal distributions of both signals which confirmed above impressions about changing relation between BHA and MUA across cortical depth.

Both, BHA and MUA distributions were nonuniform across V1 cortical depth (both KW tests, $p < 0.001$, $N = 104$), yet differed markedly (Fig. 2a-d). BHA was strongest in layers where neural firing was

sparse to undetected. It was more pronounced in the supragranular than both granular and infragranular layers (all Wilcoxon tests, $p < 0.001$). Importantly, MUA displayed the opposite pattern: it was decreased in the supragranular compared to both granular and infragranular layers (both Wilcoxon tests, $p < 0.001$). BHA magnitude ($p = 0.03$) unlike MUA ($p = 0.14$) did differ across the granular and infragranular layers. Interestingly, 70% of all cases showed strong supragranular BHA in lieu of any detectable MUA increase. The fact that the BHA and MUA have a differing laminar/temporal distributions accords with the view that these signals reflect different aspects of neural activity.

Next, we studied A1, to test whether these effects generalize to other sensory cortex. Despite differing morphology of BHA signals in V1 and A1, key aspects of differential laminar distribution of BHA and MUA generalize to A1. As in V1, event-related BHA and MUA were both observed across all three laminar compartments (Fig. 1c, f), and both had a non-uniform laminar distribution (KW tests, $p < 0.001$, $N = 26$). Critically, laminar dissociation of BHA and MUA profiles was also observed in A1 (Fig. 2e-h). BHA was stronger in the supragranular than in granular and infragranular layers (both Wilcoxon tests, $p < 0.001$). In contrast, MUA was weaker in the supragranular than in the granular and infragranular layers (both Wilcoxon tests, $p < 0.001$). The post-stimulus time interval during which BHA was increased from baseline was more sustained in the supragranular than in the granular and infragranular layers (73.5, 18.7, 20.0 ms median supra-, granular, infra-, respectively; both Wilcoxon tests, $p < 0.001$). The post-stimulus time interval during which MUA was increased from baseline was overall shorter and more sustained in deeper than in supragranular layers (15.5, 42.5, 45.5 ms median supra-, granular, infra-, respectively; both Wilcoxon tests, $p < 0.001$). Neither BHA nor MUA durations differed between granular and infragranular layers (both Wilcoxon tests, $p > 0.84$).

BHA in A1 had a clear early (0-30 ms post-stimulus) and late (31-100 ms) components, and a differential laminar distribution was noted for the magnitude of the late (KW test, $p < 0.001$) but not the early BHA (KW test, $p = 0.76$). In contrast MUA was decreased in the supragranular layers compared

to granular and infragranular layers during both time windows (all Wilcoxon tests, $p < 0.001$; Fig. 2e, g).

From both the magnitude of supragranular BHA and the proximity of supragranular current generators to the pial surface of cortex we predicted that the supragranular layers should provide the largest contribution to BHA signal at the cortical surface (typically recorded with an ECoG subdural electrode). To quantify this, we estimated percentage of variance explained by four linear regression models including the data from either individual layers or all layers together. We reasoned that the model explaining most of variance in the pial surface BHA would indicate major laminar generator of surface BHA. For both V1 and A1 penetrations, we observed that the model with supragranular signal explained more variance than models with granular or infragranular BHA alone (23.6% / 30.07%, 5.6% / 4.02%, 17.1% / 6.57% median adjusted R-squared for models including supra-, granular, infra- in V1 / A1, all Wilcoxon tests, $p < 0.003$; Fig. 3). In both V1 and A1, models including BHA from all layers explained more variance (27.0%, 31.37%; both Wilcoxon tests, $p < 0.04$) than model with supragranular BHA alone. Thus, while BHA from all laminar compartments contributes to the pial surface BHA signal, the supragranular layers are the major source.

Laminar activity profile recordings in rodents suggest that the most prominent current sink in the supragranular layers, which corresponds to the location generating the late-superficial BHA in our study, reflects Ca^{2+} dependent spiking in the apical dendrites of pyramidal neurons (21). Interestingly, the synaptically evoked Ca^{2+} signal is largely mediated by the N-methyl-D-aspartate (NMDA) receptors (22), which regulate several processes including neural plasticity (23) and dynamic shifts in neural excitability (24). Importantly, the effect of NMDA-mediated enhancement of excitability is strongest in the supragranular layers (24), consistent with preferential expression of NMDA receptors there (25). The laminar distribution of NMDA receptors and the time course of the NMDA-mediated depolarization

(slower and primarily supragranular) suggest that the later superficial BHA signal may have a strong NMDA dependence, further dissociating BHA from neuronal firing. To address this possibility, we examined the effects of systemic administration of the noncompetitive NMDA antagonist Phencyclidine (PCP) on auditory responses in A1 (N = 8 experiments, 1 animal). During control recordings (i.e., prior to PCP), stimulation elicited a sharp and transient increase in both BHA and MUA (Fig. 4). However, after PCP administration, BHA was significantly attenuated across all layers (all Wilcoxon tests, $p < 0.01$), while MUA showed no detectable difference between control and PCP (all Wilcoxon tests, $p > 0.26$). Albeit based on data from only one subject, the effects of NMDA blockade are robust and provide a pharmacological dissociation between BHA and MUA.

To test whether the spatial dissociation between BHA and MUA noted in monkeys, could be observed in humans, we used a small set of data from similar laminar probes implanted in to-be-resected tissue of the prefrontal cortex of two patients with pharmaco-resistant epilepsy during rest (Fig. S1). In short, spatial distributions of BHA and MUA were strikingly similar to those observed in monkeys with strongest BHA in the superficial electrodes and MUA in the deeper electrodes.

We identified spatial, temporal and pharmacological dissociations between BHA and MUA. BHA had two spatially and temporally distinct components; i.e., early-deep and late-superficial, observed in granular-infragranular and supragranular layers, respectively. There is a substantial spatial and temporal correspondence between MUA and the early-deep BHA component. In contrast, the MUA correlate of late-superficial BHA is much weaker, and often undetectable. The late-superficial BHA component appears to be NMDA mediated. We also found that - although BHA signals from all laminar compartments volume conduct to the pial surface, the main generators of BHA are localized in the supragranular layers where, as shown by numerous prior studies, firing is sparse (19,20,26,27). This is important, because it suggests that BHA recorded at the pial surface (e.g., with an ECoG electrode) likely over-represents signals generated in supragranular layers, while the more robust event-related

spiking activity is observed in the granular and infragranular layers. The results of laminar recording experiments in rodents (21) suggest that the large, late-superficial component may be generated by Ca^{2+} influx during apical dendritic spiking of pyramidal cells. The vulnerability of the largest (late-superficial) component of BHA signal to NMDA receptor blockade suggests that this component may index the same process.

Several critical implications of our findings for the interpretation of the BHA signal, merit further emphasis. First, BHA as recorded from pial surface reflects synaptic spiking to a relatively small extent. Our pharmacological findings (Fig. 4) link to those of Suzuki and Larkum (21) in pointing to an underlying NMDA-mediated process generating BHA. One possibility is that BHA originates from calcium-dependent spikes which are long-lasting (10-100 ms) non-synaptic events triggered by NMDA receptor mediated excitatory postsynaptic potentials (30) that have been suggested to be a mechanism for associating information carried by feedforward and feedback pathways (31). The fact that the supragranular BHA is the largest contributor to the pial surface signal suggests that BHA as typically measured in ECoG may contain a substantial representation of input from cortical feedback pathways. Importantly, the median of 33 ms (IQR = 3 ms) onset-to-onset difference between early and late supragranular BHA signals in A1 is much longer than expected for a conduction delay within a direct mono-synaptic connection between granular and supragranular layers (27). One possible explanation is that the early BHA reflects feed-forward signal propagating to L4 and then to extragranular layers, whereas the late-superficial BHA, reflects feedback from higher auditory areas to A1 which provides strong input to the supragranular layers. In feedback pathways, predictions and contextual information originating in extra-granular layers of higher-order areas are projected, to and modulate lower cortical areas. Because feedforward and feedback pathways encode different information (19), bias toward feedback circuits in ECoG-derived BHA might favor predictive and contextual information.

The idea that BHA reflects an integrative process separable from the typical action potential may help to interpret several currently unexplained observations. For example, Rich and Wallis (16) found that

BHA in the orbitofrontal cortex (OFC) although correlated with firing diverged from MUA on many dimensions and that BHA carried more information. Similarly, recordings from V1 of anesthetized cats showed that both BOLD and BHA encode stimulus intensity at a finer rate than MUA (13). BHA and local firing showed opposite changes for stimulus category preference in the ventral lateral prefrontal cortex (28). BHA and MUA also tend to temporally dissociate in the ictal core during seizure activity in human epilepsy patients (29). The relation between spikes and BHA is not uniform but shows large variability (14). Altogether, these findings are consistent with the idea that BHA reflects processes that operate in addition to local neuronal firing. This outcome imposes a caveat into the interpretation of the BHA signal, but it remains clear that the signal still has a strong relationship to neuronal firing. Improved understanding of the additional neuronal contributions to BHA makes it a richer, more useful index of brain activation.

References

1. N. Mesgarani, E. F. Chang, Selective cortical representation of attended speaker in multi-talker speech perception. *Nature* **485**, 233–236 (2012).

2. C. Tang, L. S. Hamilton, E. F. Chang, Intonational speech prosody encoding in the human auditory cortex. *Science* **801,** 797–801 (2017).

3. J. Jacobs, M. J. Kahana, Neural representations of individual stimuli in humans revealed by gamma-band electrocorticographic activity. *J Neurosci* **29,** 10203–10214 (2009).

4. T. Golan *et al.,* Increasing suppression of saccade-related transients along the human visual hierarchy. *ELife* **6,** e27819 (2017).

5. A. Flinker *et al.,* Redefining the role of Broca's area in speech. *Proc. Natl. Acad. Sci.* **112,** 2871–2875 (2015).

6. M. Leszczyński, J. Fell, N. Axmacher, Rhythmic working memory activation in the human hippocampus. *Cell Rep.* **13,** 1272–1282 (2015).

7. M. Leszczynski, J. Fell, O. Jensen, N. Axmacher, Alpha activity in the ventral and dorsal visual stream controls information flow during working memory. *BioRxiv* **180166,** (2017).

8. J. P. Lachaux, *et al.,* Progress in neurobiology high-frequency neural activity and human cognition: past , present and possible future of intracranial EEG research. *Prog. Neurobiol.* **98,** 279–301 (2012).

9. M. T. Kucewicz *et al.,* High frequency oscillations are associated with cognitive processing in human recognition memory. *Brain* **137,** 2231–2244 (2014).

10. B. Voytek *et al.,* Oscillatory dynamics coordinating human frontal networks in support of goal maintenance. *Nat. Neurosci.* **18,** 1318–1324 (2015).

11. M. Haller *et al.,* Persistent neuronal activity in human prefrontal cortex links perception and action. *Nat. Hum. Behav.* **2,** 80–91 (2018).

12. R. Mukamel *et al.,* Coupling between neuronal firing, field potentials, and FMRI in human auditory cortex. *Science* **309,** 951–954 (2005).

13. J. Niessing *et al.,* Hemodynamic signals correlate tightly with synchronized gamma oscillations. *Science* **309,** 948–951 (2005).

14. Y. Nir *et al.,* Coupling between neuronal firing rate, gamma LFP , and BOLD fMRI is related to interneuronal correlations. *Curr. Biol.* **17,** 1275–1285 (2007).

15. S. Ray, N. E. Crone, E. Niebur, P. J. Franaszczuk S. S. Hsiao, Neural correlates of high-gamma oscillations (60-200 Hz) in macaque local field potentials and their potential implications in electrocorticography. *J. Neurosci.* **28**, 11526-11536 (2008).

16. E. L. Rich, J. D. Wallis, Spatiotemporal dynamics of information encoding revealed in orbitofrontal high-gamma. *Nat. Commun.* **8,** 1139 (2017).

17. C. E. Schroeder, C. E. Tenke, S. J. Givre, J. C. Arezzo, H. G. Vaughan, Striate cortical contribution to the surface-recorded pattern-reversal VEP in the alert monkey. *Vision Res.* **31,** 1143–1157 (1991).

18. C. E. Schroeder, A. D. Mehta, S. J. A. Givre, Spatiotemporal profile of visual system activation revealed by current source density analysis in the awake macaque. *Cereb. Cortex* **8**, 575–592 (1998).

19. P. Lakatos, G. Karmos, A. D. Mehta, I. Ulbert, C. E. Schroeder, Entrainment of neuronal oscillations as a mechanism of attentional selection. *Science* **320,** 110–113 (2008).

20. Y. Kajikawa, C. E. Schroeder, How local is the local field potential? *Neuron* **72,** 847–858 (2011).

21. M. Suzuki, M. E. Larkum, Dendritic calcium spikes are clearly detectable at the cortical surface. *Nat. Commun.* **8,** 276 (2017).

22. Y. Kovalchuk, J. Eilers, J. Lisman, A. Konnerth, NMDA receptor-mediated subthreshold Ca(2+) signals in spines of hippocampal neurons. *J. Neurosci.* **20,** 1791–1799 (2000).

23. R. C. Malenka, R. A. Nicoll, NMDA-receptor-dependent synaptic plasticity: multiple forms and mechanisms. *Trends Neurosci.* **16,** 521–527 (1993).

24. C. E. Schroeder *et al.,* N-methyl-D-aspartate enhancement of phasic responses in primate neocortex. *Exp. Brain Res.* **114,** 271–278 (1997).

25. G. W. Huntley *et al.,* Distribution and synaptic localization of immunocytochemically identified NMDA receptor subunit proteins in sensory-motor and visual cortices of monkey and human. *J. Neurosci.* **14,** 3603–19 (1994).

26. S. Sakata, K. D. Harris, Laminar structure of spontaneous and sensory-evoked population activity in auditory cortex. *Neuron* **64,** 404–418 (2009).

27. C. C. H. Petersen, S. Crochet, Synaptic Computation and Sensory Processing. *Neuron* **78,** 28–48 (2013).

28. A. Wutz *et al.,* Different levels of category abstraction by different dynamics in different prefrontal areas. *Neuron* **97,** 716–726 (2018).

29. E. H. Smith *et al.,* The ictal wavefront is the spatiotemporal source of discharges during spontaneous human seizures. *Nat. Commun.* **7,** 11098 (2016).

30. M. Hausser, N. Spruston, G. J. Stuart, Diversity and dynamics of dendritic signaling. *Science* **290,** 739–744 (2000).

31. M. Larkum, A cellular mechanism for cortical associations: An organizing principle for the cerebral cortex. *Trends Neurosci.* **36,** 141–151 (2013).

Figure captions

Fig. 1 **Laminar activity profiles.** Color maps show CSD superimposed with field potentials (left) and BHA with MUA profiles (right) in V1 **(a)** and A1 **(c)** from a representative session. Vertical lines indicate sensory event. **(b, d)** show MUA-BHA cross-correlation coefficient within individual layers (left) and the lag with highest coefficient in V1 and A1, respectively. Positive values indicate that MUA leads BHA. Central mark and edges show median, 25th and 75th percentiles. **(e, f)** Z-statistics (N = 137 and 84) for V1 **(e)** and A1 **(f)** from a non-parametric pairwise test on MUA (left panel) and BHA (middle panel) relative to prestimulus baseline masked at $p < 0.05$ controlled for multiple comparisons. Right panels show an overlap (yellow) between the BHA (green) and MUA (red) laminar activity profiles for V1.

Fig. 2 **Differential laminar distribution of BHA and MUA. (a, e)** Line plots show supra-, granular and infragranular (red, green and blue lines) distributions of BHA across all sessions (N = 104, 26) in V1 **(a)** and A1 **(e)**. **(b, f)** Box plots present BHA distributions averaged across time after stimulus onset. **(c, g)** and **(d, h)** show the laminar distributions of MUA from all experiments in V1 and A1. Same plotting convention as above. Shading reflects SEM.

Fig. 3 **Laminar generators of the pial surface BHA. (a, b)** Laminar BHA recorded from supra-, granular and infragranular layers of V1 **(a)** and A1 **(b)** in a subsample of experiments (N = 31, 24, respectively) with simultaneous channels in the pial surface (gray). **(c, d)** MUA in V1 **(c)** and A1 **(d)** plotted with the same convention as above. **(e, f)** The amount of variance explained in the pial surface BHA by four different models (white, red, green, blue) in V1 **(e)** and A1 **(f).**

Fig. 4 **The effect of Phencyclidine on BHA and MUA in primary auditory cortex. (a, b)** Box plots present BHA **(a, c)** and MUA **(b, d)** before (control) and after systemic administration of PCP (N = 8). Same plotting convention.

Funding: B.R.A.I.N. - MH111439; EYE24776; DC015780; MH109429

Author contributions: ML, CES designed the study. AB, YK, AF, IU collected data. ML performed analyses. ML and CES wrote the manuscript. All authors contributed to the discussion and interpretation of findings, and edited the manuscript.

Competing interests: Authors declare no competing interests.

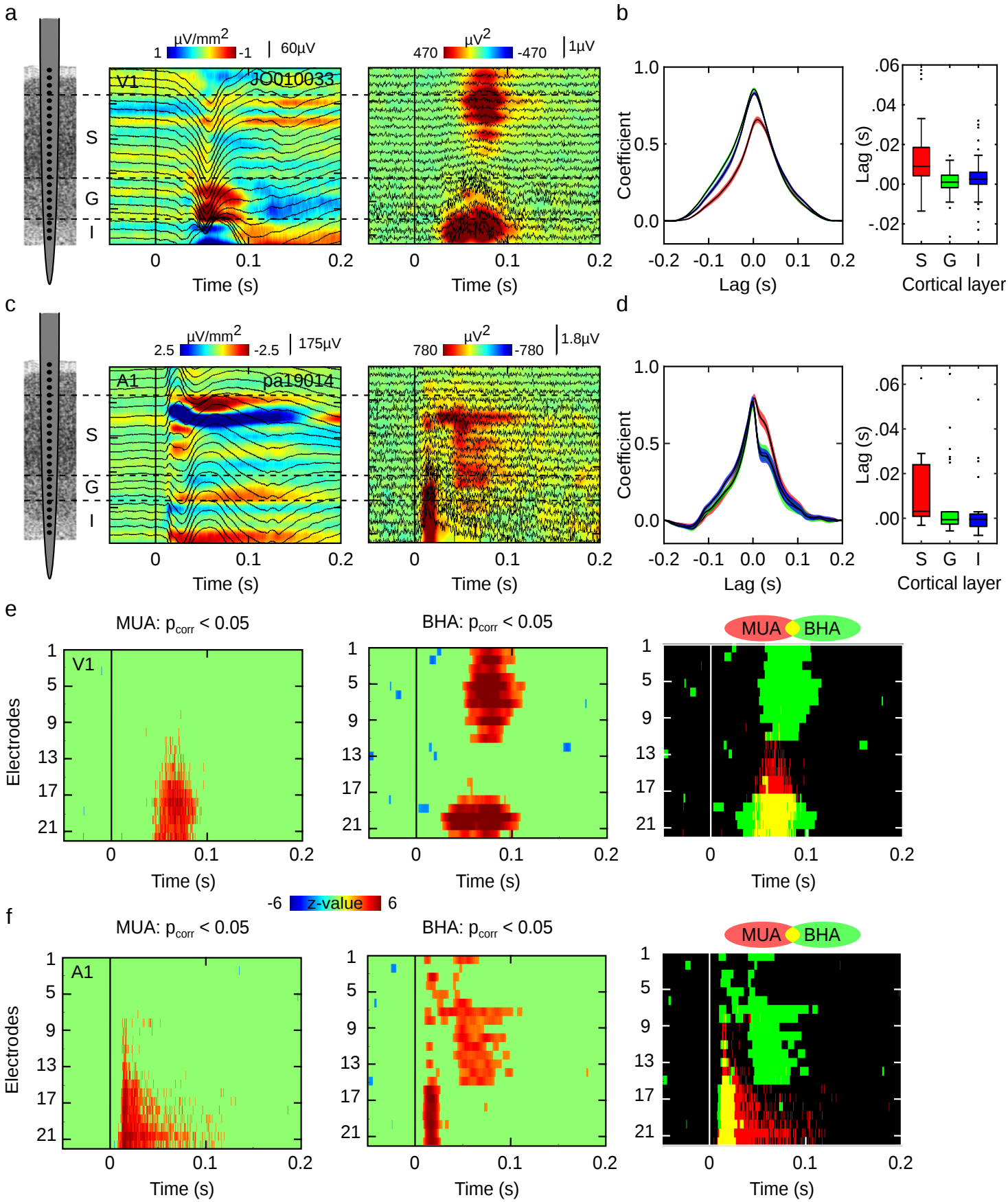
a
μV/mm2
1
-1
60μV
μV2
470
-470
1μV
V1
JO010033
S
G
I
0
0.1
0.2
Time (s)
b
Coefficient
1.0
0.5
0.0
-0.2
-0.1
0.0
0.1
0.2
Lag (s)
.06
.04
.02
.00
-.02
Lag (s)
S
G
I
Cortical layer
c
2.5
-2.5
175μV
780
-780
1.8μV
A1
pa19014
d
.00
e
MUA: pcorr < 0.05
BHA: pcorr < 0.05
MUA
BHA
Electrodes
1
5
9
13
17
21
-6
z-value
6
f

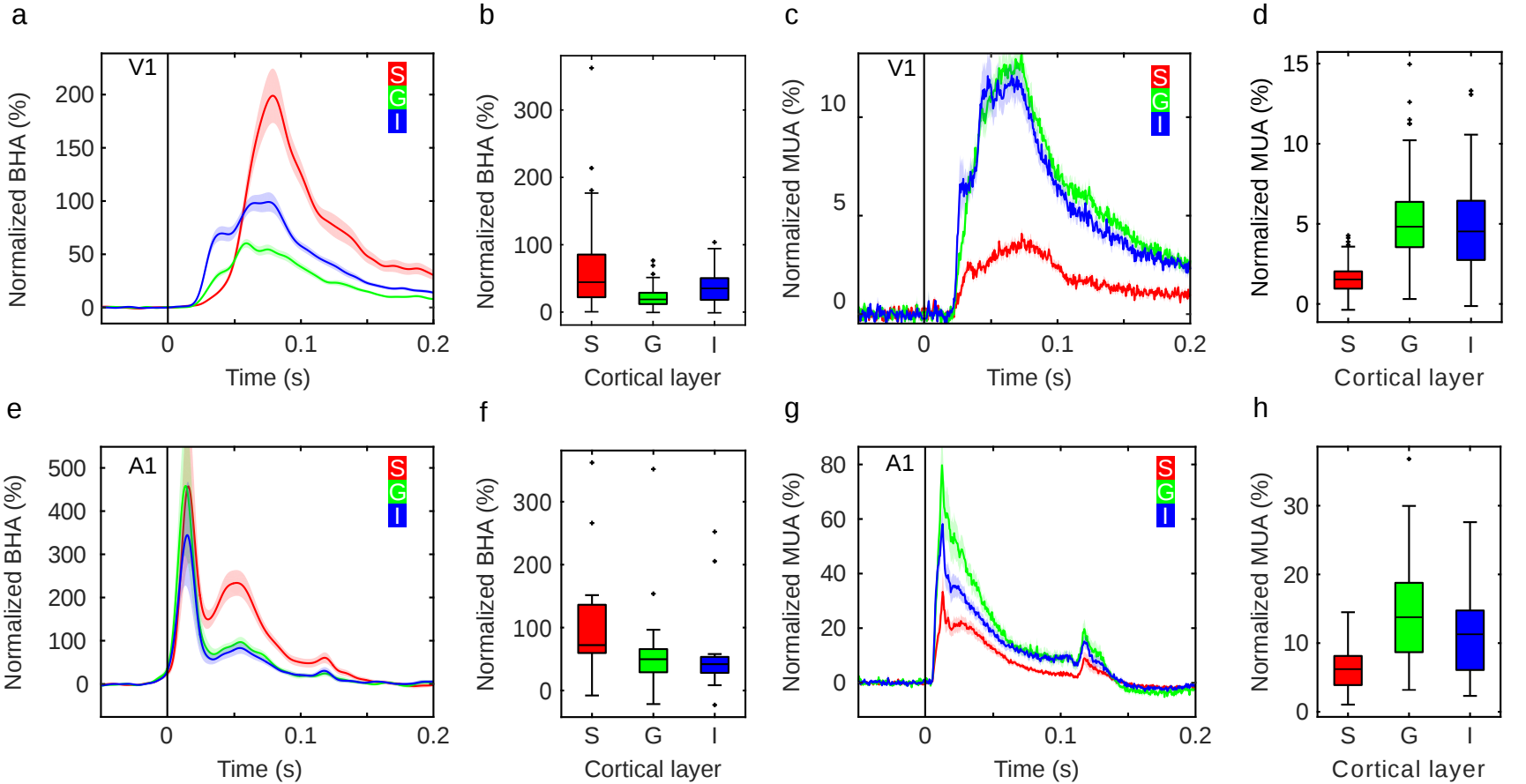
a
V1
S
G
I
Normalized BHA (%)
Time (s)
b
Normalized BHA (%)
Cortical layer
c
V1
Normalized MUA (%)
Time (s)
d
Normalized MUA (%)
Cortical layer
e
A1
Normalized BHA (%)
Time (s)
f
Normalized BHA (%)
Cortical layer
g
A1
Normalized MUA (%)
Time (s)
h
Normalized MUA (%)
Cortical layer

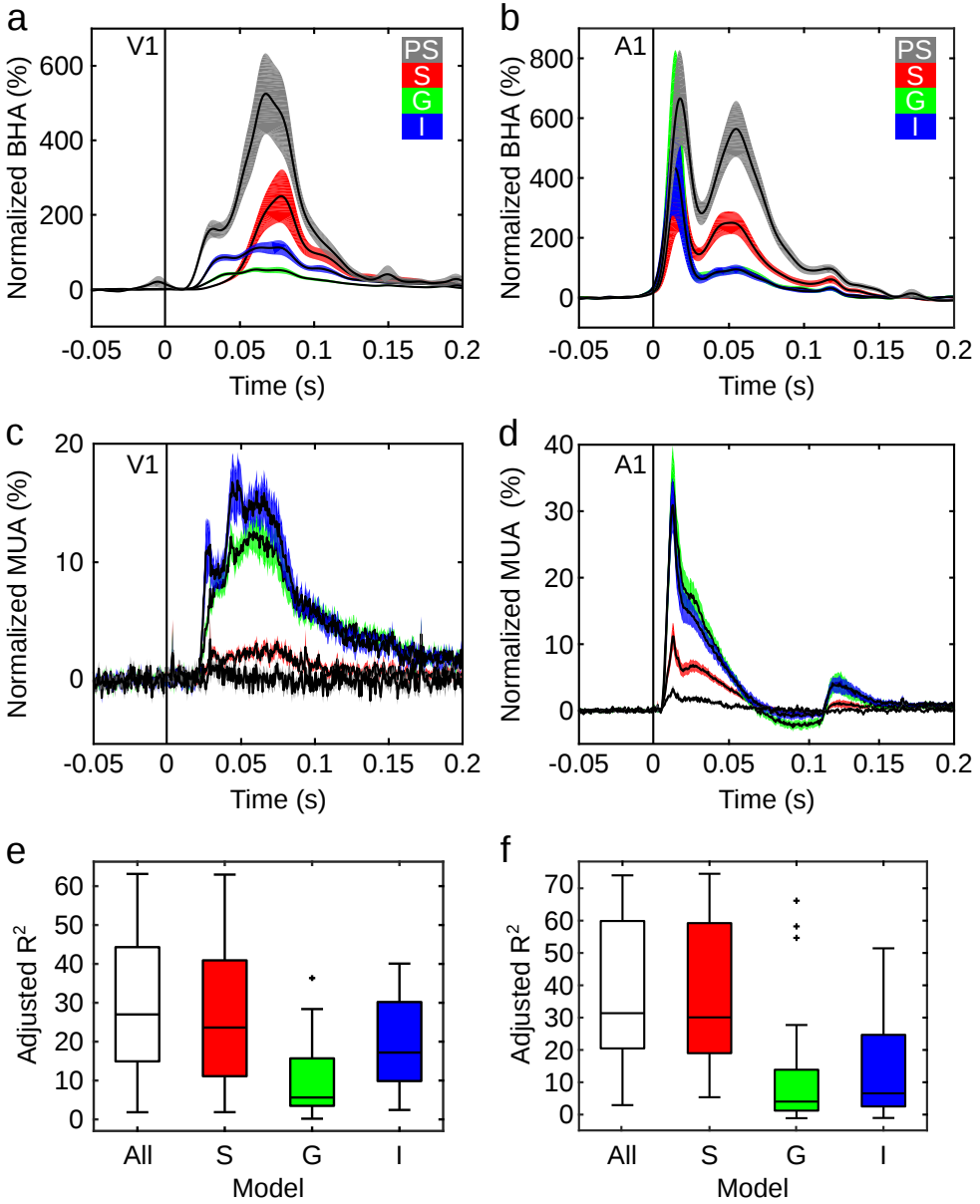
a
V1
PS
S
G
I
Normalized BHA (%)
600
400
200
0
-0.05
0
0.05
0.1
0.15
0.2
Time (s)
b
A1
PS
S
G
I
Normalized BHA (%)
800
600
400
200
0
-0.05
0
0.05
0.1
0.15
0.2
Time (s)
c
V1
Normalized MUA (%)
20
10
0
-0.05
0
0.05
0.1
0.15
0.2
Time (s)
d
A1
Normalized MUA (%)
40
30
20
10
0
-0.05
0
0.05
0.1
0.15
0.2
Time (s)
e
Adjusted R2
60
50
40
30
20
10
0
All
S
G
I
Model
f
Adjusted R2
70
60
50
40
30
20
10
0
All
S
G
I
Model

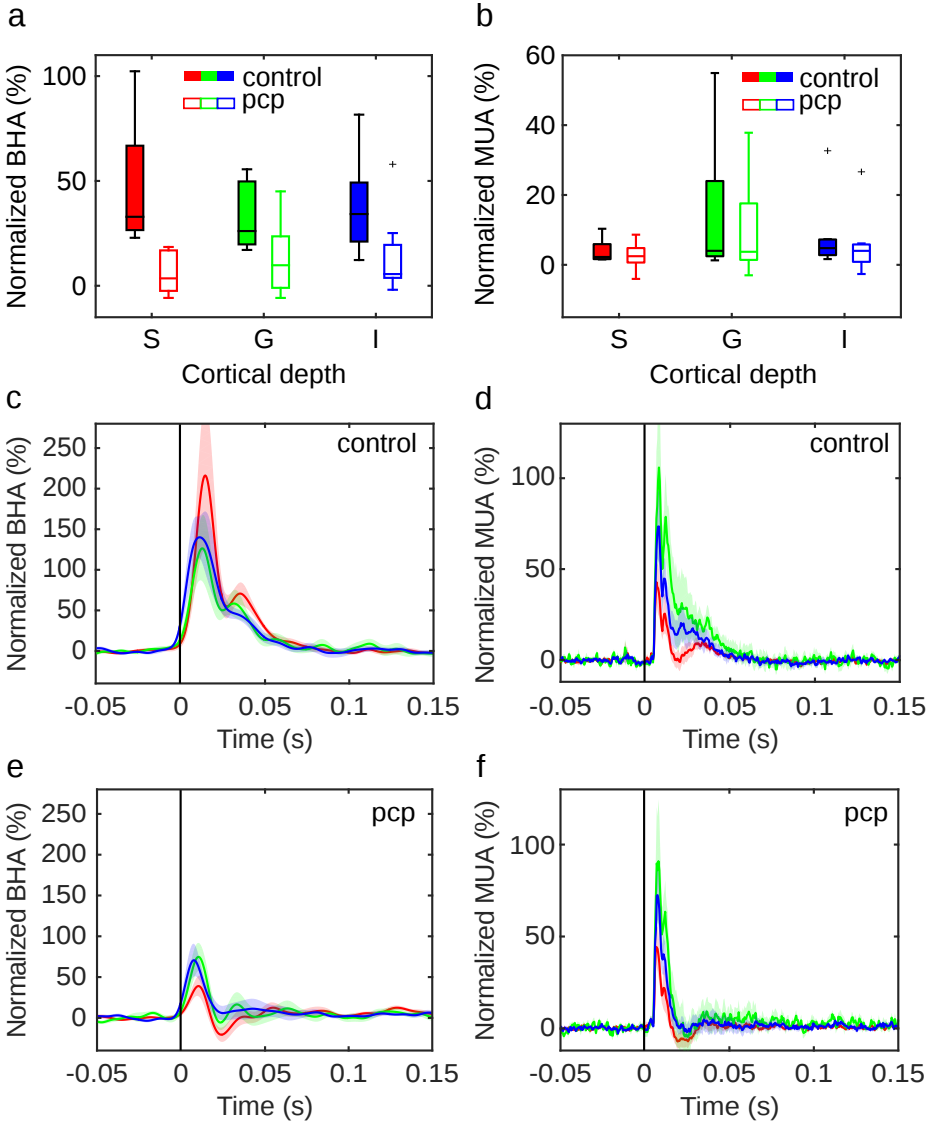
a
Normalized BHA (%)
100
50
0
control
pcp
S
G
I
Cortical depth
b
Normalized MUA (%)
60
40
20
0
control
pcp
S
G
I
Cortical depth
c
Normalized BHA (%)
250
200
150
100
50
0
control
-0.05
0
0.05
0.1
0.15
Time (s)
d
Normalized MUA (%)
100
50
0
control
-0.05
0
0.05
0.1
0.15
Time (s)
e
Normalized BHA (%)
250
200
150
100
50
0
pcp
-0.05
0
0.05
0.1
0.15
Time (s)
f
Normalized MUA (%)
100
50
0
pcp
-0.05
0
0.05
0.1
0.15
Time (s)